JCI insight

Inhibiting myeloid-derived suppressor cell trafficking enhances T cell immunotherapy

Lillian Sun, … , John Zebala, Clint T. Allen

JCI Insight. 2019;4(7):e126853. https://doi.org/10.1172/jci.insight.126853.

Research Article Oncology

Recruitment of myeloid-derived suppressor cells (MDSCs) into tumors induces local immunosuppression in carcinomas. Here, we assessed whether SX-682, an orally bioavailable small-molecule inhibitor of CXCR1 and CXCR2, could block tumor MDSC recruitment and enhance T cell activation and antitumor immunity following multiple forms of immunotherapy. $CXCR2^+$ neutrophilic MDSCs (PMN-MDSCs) were the most abundant myeloid cell subset within oral and lung syngeneic carcinomas. PMN-MDSCs demonstrated greater suppression of tumor-infiltrating lymphocyte killing of targets compared with macrophages. SX-682 significantly inhibited trafficking of PMN-MDSCs without altering CXCR2 ligand expression. Trafficking of $CXCR1^+$ macrophages was unaltered, possibly due to coexpression of CSF1R. Reduced PMN-MDSC tumor infiltration correlated with enhanced accumulation of endogenous or adoptively transferred T cells. Accordingly, tumor growth inhibition or the rate of established tumor rejection following programed death–axis (PD-axis) immune checkpoint blockade or adoptive cell transfer of engineered T cells was enhanced in combination with SX-682. Despite CXCR1/2 expression on tumor cells, SX-682 appeared to have little direct antitumor effect on these carcinoma models. These data suggest that tumor-infiltrating $CXCR2^+$ PMN-MDSCs may prevent optimal responses following both PD-axis immune checkpoint blockade and adoptive T cell transfer therapy. Abrogation of PMN-MDSC trafficking with SX-682 enhances T cell–based immunotherapeutic efficacy and may be of benefit to patients with MDSC-infiltrated cancers.

JCI insight

RESEARCH ARTICLE

Inhibiting myeloid-derived suppressor cell trafficking enhances T cell immunotherapy

Lillian Sun,[1] Paul E. Clavijo,[1] Yvette Robbins,[1] Priya Patel,[1] Jay Friedman,[1] Sarah Greene,[1] Rita Das,[2] Chris Silvin,[2] Carter Van Waes,[2] Lucas A. Horn,[3] Jeffrey Schlom,[3] Claudia Palena,[3] Dean Maeda,[4] John Zebala,[4] and Clint T. Allen[1,5]

[1]Translation Tumor Immunology Program and [2]Tumor Biology Section, National Institute on Deafness and Other Communication Disorders, NIH, Bethesda, Maryland, USA. [3]Laboratory of Tumor Immunology and Biology, Center for Cancer Research, National Cancer Institute, NIH, Bethesda, Maryland, USA. [4]Syntrix Pharmaceuticals, Auburn, Washington, USA. [5]Department of Otolaryngology-Head and Neck Surgery, Johns Hopkins School of Medicine, Baltimore, Maryland, USA.

Recruitment of myeloid-derived suppressor cells (MDSCs) into tumors induces local immunosuppression in carcinomas. Here, we assessed whether SX-682, an orally bioavailable small-molecule inhibitor of CXCR1 and CXCR2, could block tumor MDSC recruitment and enhance T cell activation and antitumor immunity following multiple forms of immunotherapy. CXCR2$^+$ neutrophilic MDSCs (PMN-MDSCs) were the most abundant myeloid cell subset within oral and lung syngeneic carcinomas. PMN-MDSCs demonstrated greater suppression of tumor-infiltrating lymphocyte killing of targets compared with macrophages. SX-682 significantly inhibited trafficking of PMN-MDSCs without altering CXCR2 ligand expression. Trafficking of CXCR1$^+$ macrophages was unaltered, possibly due to coexpression of CSF1R. Reduced PMN-MDSC tumor infiltration correlated with enhanced accumulation of endogenous or adoptively transferred T cells. Accordingly, tumor growth inhibition or the rate of established tumor rejection following programed death–axis (PD-axis) immune checkpoint blockade or adoptive cell transfer of engineered T cells was enhanced in combination with SX-682. Despite CXCR1/2 expression on tumor cells, SX-682 appeared to have little direct antitumor effect on these carcinoma models. These data suggest that tumor-infiltrating CXCR2$^+$ PMN-MDSCs may prevent optimal responses following both PD-axis immune checkpoint blockade and adoptive T cell transfer therapy. Abrogation of PMN-MDSC trafficking with SX-682 enhances T cell–based immunotherapeutic efficacy and may be of benefit to patients with MDSC-infiltrated cancers.

Introduction

Multiple mechanisms of escape from T cell immunity exist within carcinomas including chemokine-driven recruitment of immunosuppressive cells into the tumor microenvironment (TME) (1). In many squamous cell carcinomas (SCCs), this occurs in part due to common genomic alterations such as chromosome 3q copy number gain and overexpression of ΔNp63 that drives myeloid and lymphoid chemokine expression (2–5). These tumor-secreted chemokines drive chemokine receptor–mediated chemotaxis of different immune populations into tumors (6). A subset of recruited myeloid cells termed myeloid-derived suppressor cells (MDSCs) inhibit T cell function through well-defined mechanisms including arginase and inducible nitric oxide synthase (iNOS) expression and production of immunosuppressive cytokines such as transforming growth factor β (TGF-β) and interleukin-10 (IL-10) (7, 8). Tumor accumulation of 2 phenotypically and functionally distinct subtypes of MDSCs, neutrophilic MDSCs (PMN-MDSCs) and monocytic MDSCs (M-MDSCs), appears to be tumor type dependent (7, 8). Peripheral or tumor accumulation of either MDSC subset correlates with poorer clinical responses to programmed death–axis (PD-axis) immune checkpoint blockade (9, 10).

Depletion or pharmacologic inhibition of MDSCs enhances responses to PD-axis immune checkpoint blockade in syngeneic models of SCC and adenocarcinoma (11–14). Strategies to deplete MDSCs are not easily translated clinically, and small-molecule inhibitors blocking MDSC function may alter the function of effector

Conflict of interest: DM and JZ are paid employees of Syntrix Pharmaceuticals.

Submitted: December 17, 2018
Accepted: February 21, 2019
Published: April 4, 2019.

Reference information: *JCI Insight*. 2019;4(7):e126853. https://doi.org/10.1172/jci.insight.126853.

immune cells (15). As an alternative treatment strategy, novel small-molecule chemokine receptor inhibitors may provide the opportunity to abrogate trafficking of hematopoietic cells with high specificity (16).

Here, we demonstrated selective expansion and tumor trafficking of CXCR2$^+$ PMN-MDSCs that suppress effector function of antigen-specific tumor-infiltrating lymphocytes (TILs) in syngeneic models of oral and lung SCC. SX-682, a novel small-molecule allosteric inhibitor of CXCR1 and CXCR2, abrogated tumor accumulation of PMN-MDSCs and enhanced the efficacy of both PD-axis immune checkpoint blockade and adoptive cell transfer of engineered T cells. These results indicate that local immunosuppression mediated by PMN-MDSCs may limit responses to both immune checkpoint blockade and adoptive cell transfer and provide the preclinical rationale for combining chemokine receptor inhibitors to selectively abrogate CXCR2$^+$ cell trafficking with T cell–based cancer immunotherapy.

Results

Carcinomas harbor a diversity of immune cell lineages within the TME (1, 2). We first assessed constituency of the myeloid compartment in MOC1 oral carcinoma and Lewis lung carcinoma (LLC) tumors grown in wild-type B6 mice (Figure 1, A and B) with flow cytometry. Ly6G^{hi}Ly6C^{int} myeloid cells and F4/80$^+$ macrophages represented the most abundant myeloid cell types within both models. These cells were individually sorted and assessed for their ability to suppress tumor cell killing by cultured TILs (Figure 1, C and D). In both models, at a similar myeloid to T cell ratio as that found in vivo (3:1 myeloid/T cell), Ly6G^{hi}Ly6C^{int} myeloid cells suppressed the ability of TILs cultured from each tumor to kill the cell line from which the tumor was generated (tumor antigen–specific killing). Thus, these Ly6G^{hi} myeloid cells are immunosuppressive and represent granulocytic MDSCs (PMN-MDSCs) (17). To verify the immunosuppressive capacity of the tumor-infiltrating PMN-MDSCs, their ability to suppress IFN-γ production by anti-CD3/anti-28 mAb–stimulated TILs was assessed via flow cytometry. PMN-MDSCs from both models significantly suppressed the ability of TILs to produce IFN-γ at the same 3:1 ratio (Supplemental Figure 1; supplemental material available online with this article; https://doi.org/10.1172/jci.insight.126853DS1). MOC1 F4/80$^+$ macrophages suppressed TIL function to a lesser degree compared with PMN-MDSCs, and LLC F4/80$^+$ macrophages did not appear to inhibit TIL function. The M1/M2 macrophage phenotype, as assessed by cell surface MHC class II and CD206 expression, was evaluated by flow cytometry. Macrophages infiltrating MOC1 tumors displayed an M1/M2 ratio less than 1, correlating to some degree of TIL suppressive capacity, whereas macrophages infiltrating LLC tumors displayed an M1/M2 ratio greater than 1 (Supplemental Figure 2).

To evaluate putative chemokine receptors that could be responsible for chemotaxis of these myeloid cells into the TME, peripheral immune cell subsets were evaluated for CXCR1 and CXCR2 expression. Expression of these chemokine receptors on myeloid cells within the TME is of little value since these receptors undergo receptor-mediated endocytosis upon ligation (11, 18). In both models, CXCR1 appeared to be highly expressed on peripheral F4/80$^+$ macrophages and CXCR2 was highly expressed on peripheral PMN-MDSCs (Figure 1, E and F). Together, these data suggested that CXCR2$^+$ PMN-MDSCs represent the most abundant immunosuppressive myeloid cell population in MOC1 and LLC tumors.

SX-682 is an orally bioavailable small-molecule inhibitor of CXCR1 and CXCR2 (14). Mice bearing MOC1 or LLC tumors were treated with chow containing SX682 and evaluated for alteration of tumor growth and myeloid cell infiltration. Significant accumulation of myeloid cells within MOC1 tumors occurs between 10 and 20 days after tumor initiation (11). Initiation of treatment on day 10 or 20 is designed to assess the impact of chemokine receptor inhibition before or after accumulation of myeloid cells within the TME. SX-682 monotherapy beginning 10 or 20 days after tumor initiation did not alter primary tumor growth in either model (Figure 2, A and B). Treatment with SX-682 significantly abrogated day 25 tumor infiltration of CXCR2$^+$ PMN-MDSCs, whereas tumor infiltration of CXCR2$^-$Ly6G^{lo}Ly6C^{hi} myeloid cells was unaltered (Figure 2, C and D). SX-682 did not alter Ki67 positivity of tumor-infiltrating PMN-MDSCs, suggesting this decrease in number was not due to inhibition of PMN-MDSC expansion within the tumor (Supplemental Figure 3). SX-682 treatment starting on day 10 resulted in greater accumulation of PMN-MDSCs in the spleen but not the bone marrow, suggesting that signaling through CXCR2 is important for PMN-MDSC trafficking from the periphery to the tumor. Neither the accumulation nor M1/M2 phenotype of tumor-infiltrating macrophages was altered by SX-682 treatment (Supplemental Figure 4, A–C). This may be due to coexpression of other myeloid chemokine receptors such as colony-stimulating factor-1 receptor (CSF1R) expressed on peripheral macrophages but not PMN-MDSCs (Supplemental Figure 4D).

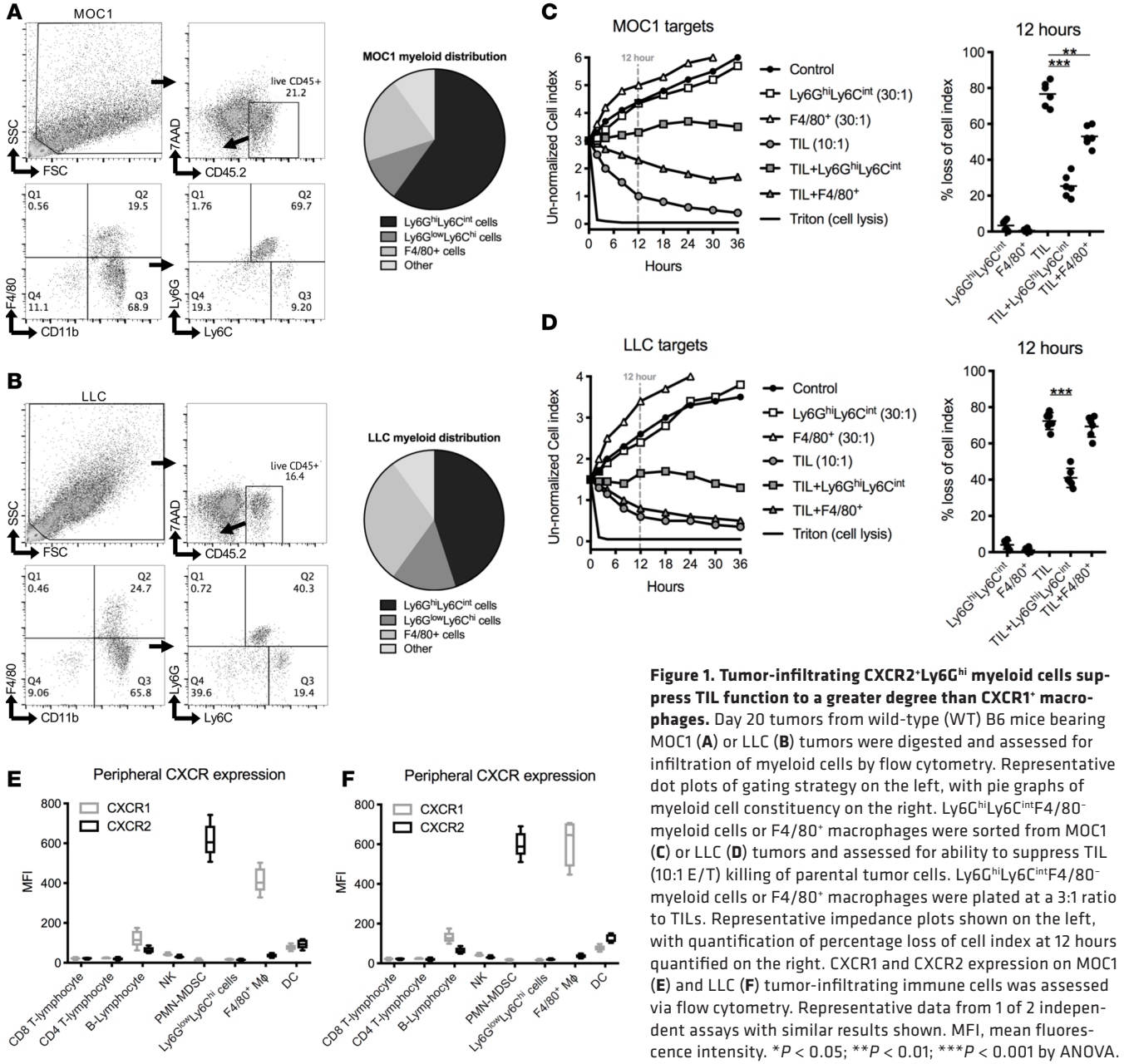

Figure 1. Tumor-infiltrating CXCR2$^+$Ly6G^{hi} myeloid cells suppress TIL function to a greater degree than CXCR1$^+$ macrophages. Day 20 tumors from wild-type (WT) B6 mice bearing MOC1 (**A**) or LLC (**B**) tumors were digested and assessed for infiltration of myeloid cells by flow cytometry. Representative dot plots of gating strategy on the left, with pie graphs of myeloid cell constituency on the right. Ly6G^{hi}Ly6C^{int}F4/80$^-$ myeloid cells or F4/80$^+$ macrophages were sorted from MOC1 (**C**) or LLC (**D**) tumors and assessed for ability to suppress TIL (10:1 E/T) killing of parental tumor cells. Ly6G^{hi}Ly6C^{int}F4/80$^-$ myeloid cells or F4/80$^+$ macrophages were plated at a 3:1 ratio to TILs. Representative impedance plots shown on the left, with quantification of percentage loss of cell index at 12 hours quantified on the right. CXCR1 and CXCR2 expression on MOC1 (**E**) and LLC (**F**) tumor-infiltrating immune cells was assessed via flow cytometry. Representative data from 1 of 2 independent assays with similar results shown. MFI, mean fluorescence intensity. *P < 0.05; **P < 0.01; ***P < 0.001 by ANOVA. n/s, nonsignificant.

IL-8 represents the major cognate ligand for CXCR2 in patients with cancer and in human xenograft models that express human IL-8 (6, 19). In syngeneic mouse models of carcinoma, the IL-8 homolog CXCL1 is the dominant biologically relevant ligand for CXCR2 (11, 20–22). We investigated whether SX-682 treatment altered tumor production of CXCL1 as an alternative explanation for inhibition of recruitment of CXCR2$^+$ PMN-MDSCs (Supplemental Figure 5, A and B). Tumor cell production of CXCL1 in vitro was unaltered by SX-682 exposure. Whole tumor accumulation of CXCL1 in vivo in MOC1 and LLC tumors was significantly greater than oral mucosa and normal lung, respectively, and not diminished with SX-682 treatment. Plasma accumulation of CXCL1 was greater in tumor-bearing mice compared with naive for both models and increased following SX-682 treatment. These data suggested that reduced tumor accumulation of CXCR2$^+$ PMN-MDSCs was not due to inhibition of CXCL1 expression.

We next investigated whether inhibition of PMN-MDSC recruitment with SX-682 altered accumulation of TILs. Day 25 MOC1 and LLC tumors both displayed greater accumulation of PD-1$^+$CD137$^+$CD8$^+$

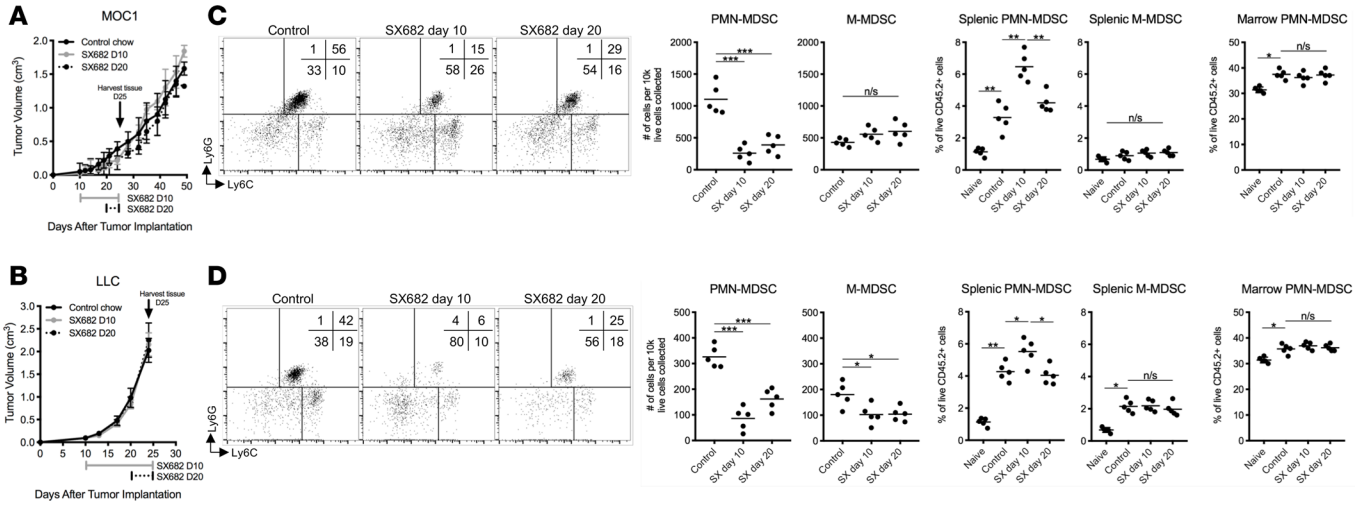

Figure 2. SX-682 monotherapy abrogates CXCR2⁺ PMN-MDSC tumor infiltration. WT B6 mice bearing MOC1 (**A**) or LLC (**B**) tumors were treated with SX-682 chow starting on either day 10 or day 20 after implantation and followed for tumor growth. Summary growth curves shown (n = 10/group). Day 25 tumors, spleens, and bone marrow harvested from MOC1 (**C**) or LLC (**D**) tumor-bearing mice treated with SX-682 chow beginning on day 10 or 20 after tumor implantation or control chow were assessed for infiltration/accumulation of PMN-MDSCs or Ly6G^{lo}Ly6C^{hi} myeloid cells by flow cytometry (n = 5/group). Representative dot plots on the left, with quantification of myeloid cells within each tissue compartment on the right. Representative data from 1 of 2 independent assays with similar results shown. n/s, nonsignificant. *P < 0.05; **P < 0.01; ***P < 0.001 by ANOVA.

TILs when SX-682 treatment was administered on day 10 but not when SX-682 was administered on day 20 (Figure 3, A and B). Within both tumor models, tumor cells displayed greater expression of PD-L1 on day 10 after SX-682 treatment (Figure 3, C and D). We hypothesized that this increase was due to increased IFN production from CD8⁺ T cells, consistent with the concept of adaptive immune resistance (23). Antibody depletion of CD8⁺ T cells abrogated the increased tumor cell PD-L1 expression (Figure 3, E and F), consistent with this hypothesis.

Increased expression of PD-1 on CD8⁺ TILs and PD-L1 on tumor cells suggested that PD-axis signaling could be limiting T cell effector function following SX-682 treatment. Thus, we hypothesized that inhibiting tumor infiltration of PMN-MDSCs with SX-682 starting on day 10 could enhance the antitumor effects of systemic PD-axis immune checkpoint blockade. Although treatment with SX-682 or anti–PD-1 mAb alone produced no significant tumor growth inhibition in either model, the combination treatment of SX-682 and PD-1 mAb significantly enhanced tumor growth delay and survival in both models and induced complete tumor rejection in 20% of mice bearing MOC1 tumors (Figure 4, A and B). Tumor growth inhibition and/or rejection induced by SX-682 and PD-1 mAb combination therapy was abrogated in mice depleted of CD8⁺ cells, strongly supporting a CD8⁺ T cell–dependent mechanism (Figure 4, C and D). Treatment with SX-682 did not directly alter the immunosuppressive capacity of tumor-infiltrating PMN-MDSCs (Supplemental Figure 6), suggesting that the enhanced responses to PD-1 mAb in both models is primarily a result of abrogated PMN-MDSC tumor infiltration.

As SX-682 enhanced tumor infiltration of endogenous T cells in wild-type mice, we hypothesized that inhibition of tumor PMN-MDSC infiltration could enhance tumor infiltration of adoptively transferred engineered T cells. RAG1-deficient mice bearing MOC1 or LLC tumors engineered to express $OVA_{257–264}$ (SIINFEKL) were treated with adoptive transfer of ex vivo–expanded OT-I cytotoxic T lymphocytes (CTLs) with or without SX-682. Following SX-682 treatment alone, tumor accumulation of PMN-MDSCs was abrogated in both models (Figure 5, A and B), similar to findings observed in wild-type mice. This reduction in PMN-MDSCs in RAG1-deficient mice correlated with enhanced tumor infiltration of adoptively transferred T cells administered 4 days after initiation of SX-682 treatment (Figure 5, C and D). To investigate whether this increase in TIL infiltration was biologically relevant, RAG1-deficient mice bearing SIINFEKL-positive MOC1 or LLC tumors were treated with a combination of SX-682 and OT-I adoptive cell transfer (Figure 6, A and B). Treatment with SX-682 chow alone induced no tumor growth inhibition, and treatment with OT-I adoptive cell transfer alone induced some degree of growth delay in both models. However, combination treatment induced significant growth delay in MOC1 tumors and promoted complete rejection of 70% of LLC tumors, with significant growth delay in the remaining, resulting

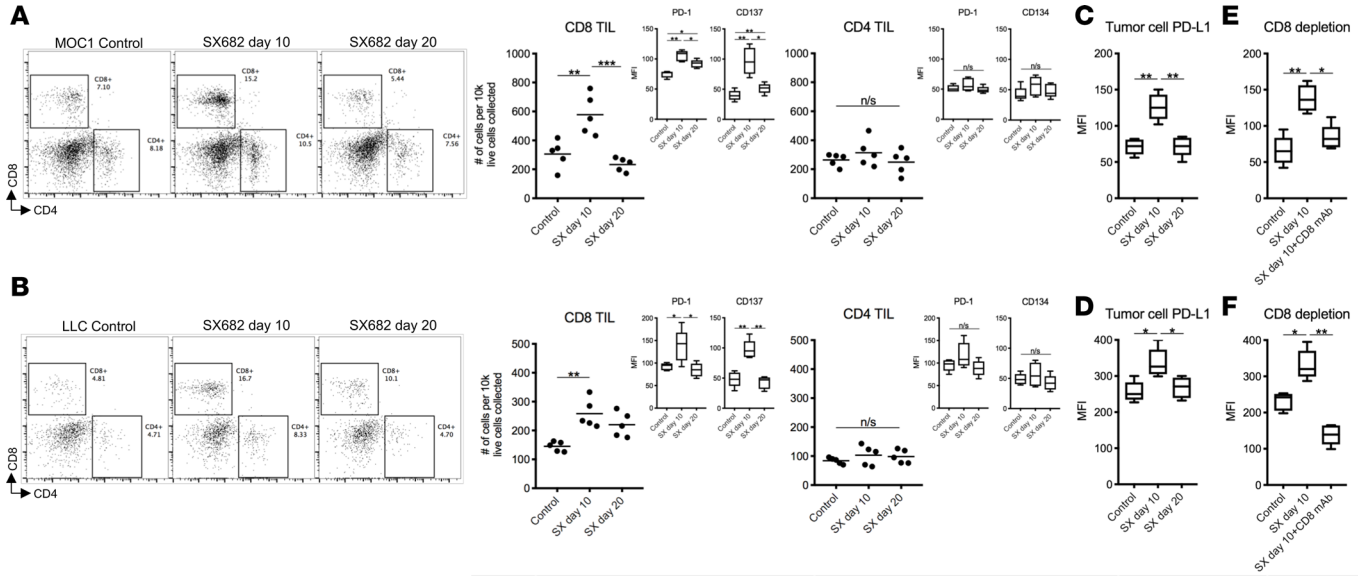

Figure 3. SX-682 treatment results in enhanced TIL infiltration and tumor cell PD-L1 expression. Day 25 tumors from mice bearing MOC1 (**A**) or LLC (**B**) tumors were treated with SX-682 chow starting on either day 10 or day 20 after implantation, then digested and assessed for infiltration of TILs by flow cytometry. Representative dot plots of live CD45.2$^+$ cells on the left with quantification of CD8$^+$ and CD4$^+$ TILs on the right. Inset is PD-1 and CD137 expression on TILs. From the same tumors, PD-L1 expression on MOC1 (**C**) or LLC (**D**) CD45.2$^-$CD31$^-$PDGFR$^-$ tumor cells were assessed with flow cytometry. PD-L1 expression on day 25 CD45.2$^-$CD31$^-$PDGFR$^-$ MOC1 (**E**) and LLC (**F**) tumor cells was assessed following treatment on day 10 with SX-682 with or without antibody depletion of CD8$^+$ cells (clone YTS 169.4, 200 μg i.p. twice weekly). Representative data from 1 of 2 independent assays with similar results shown. n/s, nonsignificant. $^*P < 0.05$; $^{**}P < 0.01$; $^{***}P < 0.001$ by ANOVA.

in significantly prolonged survival. These data suggested that, in addition to enhancing antitumor efficacy of PD-axis immune checkpoint blockade, abrogation of PMN-MDSC tumor infiltration with SX-682 can enhance the therapeutic efficacy of adoptively transferred T cells.

We additionally explored whether SX-682 modulated any direct antitumor effects. MOC1 and LLC cells expressed both CXCR1 and CXCR2 in vitro to a greater degree than oral or lung epithelial cells in vivo (Figure 7A). Treatment of mice bearing MOC1 or LLC tumors with SX-682 beginning 10 or 20 days after tumor initiation did not alter CXCR1 or CXCR2 expression on tumor cells in vivo (Figure 7B). Assessed by impedance analysis, exposure of MOC1 or LLC cells to increasing doses of SX-682 as high as 5 μM did not alter tumor cell viability or proliferation (Figure 7C), nor did it induce evidence of apoptosis (Figure 7D). Exposure of MOC1 or LLC tumor cells to a recombinant murine CXCL1 chemokine gradient did not induce migration or invasion through an extracellular matrix (ECM). SX-682 treatment did modestly inhibit ECM invasion in response to 10% serum (Figure 7E). Lastly, SX-682 treatment did not directly enhance antigen-specific OT-I CTL killing of MOC1 or LLC tumor cells expressing SIINFEKL in vitro (Figure 7F). Cumulatively, these data suggested that the enhanced therapeutic efficacy of PD-axis immune checkpoint blockade and OT-I adoptive cell transfer following SX-682 treatment was primarily due to reduced tumor infiltration of immunosuppressive CXCR2$^+$ PMN-MDSCs and not due to reduced CXCR2 ligand expression, abrogated PMN-MDSC suppressive capacity, or direct antitumor cell effects.

Discussion

PD-axis immune checkpoint blockade aims to reverse adaptive immune resistance associated with IFN-driven PD-L1 ligation of PD-1 on TILs but fails to induce objective responses in the majority of treated patients as a monotherapy (23). An alternative immunotherapeutic approach, adoptive T cell transfer, presumes that antigen-specific TILs are exhausted, difficult to rescue with immune checkpoint blockade, and therefore need to be replaced (24). Each of these immunotherapeutic approaches demonstrate clinical activity in a subset of treated patients with recurrent/metastatic malignancy (25–28). While differing in mechanism, both approaches may be limited by ineffective tumor penetrance of T cells and local T cell immunosuppression within the TME (29). Here, we demonstrated enhanced activity of both anti–PD-1 mAb immune checkpoint blockade and engineered adoptive T cell transfer immunotherapy

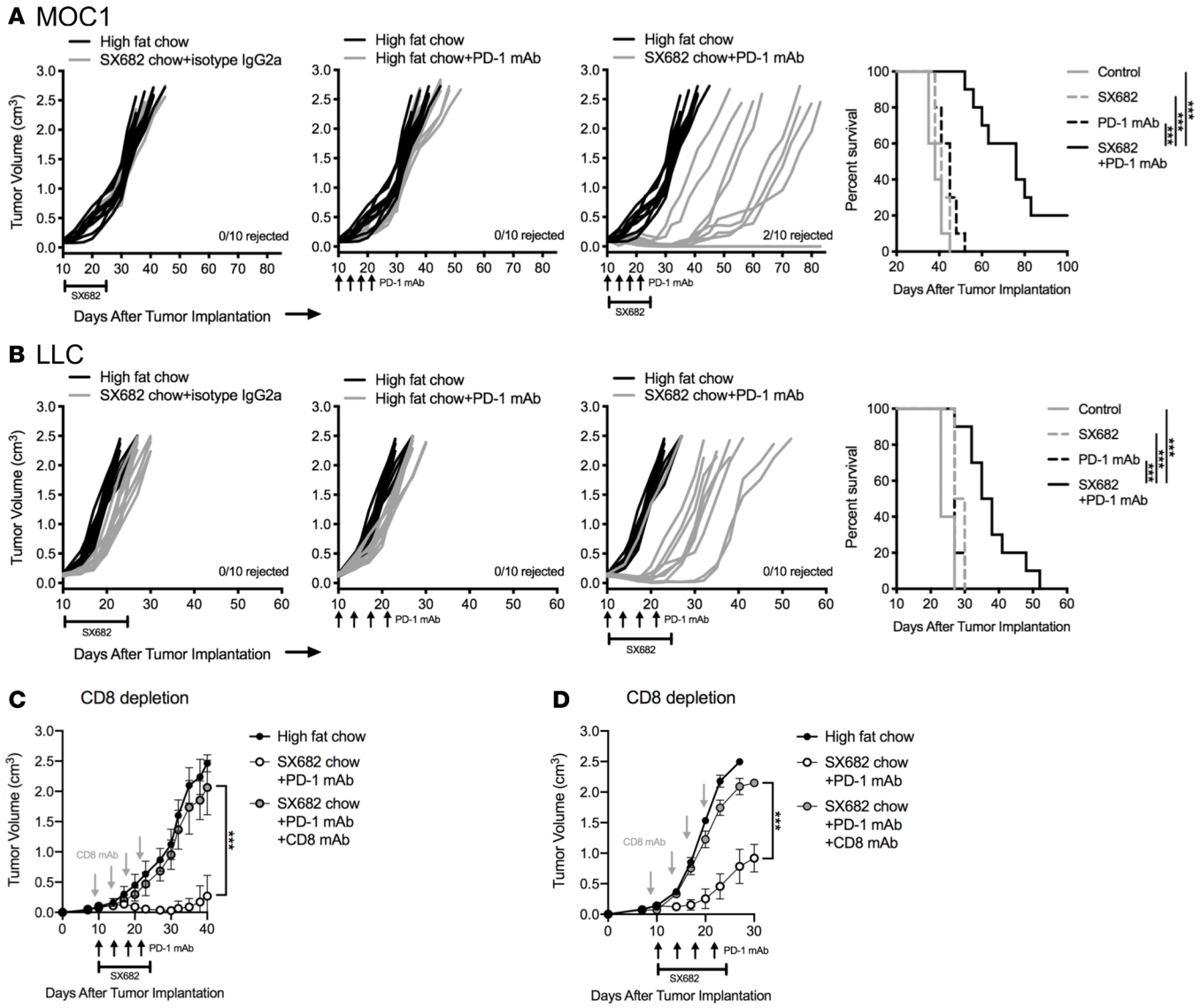

Figure 4. SX-682 enhances tumor control or rejection following PD-1 blockade. WT B6 mice bearing established MOC1 (**A**) or LLC (**B**) tumors were treated with SX-682 or control chow and PD-1 mAb (200 μg i.p. twice weekly for a total of 4 injections) or isotype control IgG2a mAb, alone or in combination, starting on day 10 and followed for primary tumor growth (left) and survival (right). ***$P < 0.001$ by log-rank (Mantel-Cox) analysis. Mice bearing established MOC1 (**C**) or LLC (**D**) tumors (n = 8/group) were treated with a combination of SX-682 and PD-1 mAb with or without antibody depletion of $CD8^+$ cells (clone YTS 169.4, 200 μg i.p. twice weekly). Representative data from 1 of 2 independent assays with similar results shown. ***$P < 0.001$ by Student's t test between tumor volumes on final day of measurement.

through small-molecule inhibition of $CXCR2^+$ PMN-MDSC chemotaxis. Blocking PMN-MDSC tumor trafficking enhanced endogenous and adoptively transferred T cell accumulation within tumors and led to significantly enhanced tumor growth inhibition or rate of tumor rejection when combined with immunotherapy. Mechanistically, this appeared to be due exclusively to inhibition of PMN-MDSC trafficking, as PMN-MDSC suppressive capacity and proliferation as well as tumor CXCL1 expression were not altered. Further, there appeared to be no direct antitumor effects with CXCR1/2 blockade in these models of oral and lung SCC.

Previous work using CXCR2-deficient mice has demonstrated an important role for CXCR2 signaling and neutrophilic cell chemotaxis in models of head and neck, lung, renal, colon, and pancreatic cancer (21, 30–34). Although the use of CXCR2-deficient mice allowed insight into the role of CXCR2 signaling and neutrophilic cell chemotaxis in tumorigenesis, they did not allow the study of therapeutic manipulation of CXCR2 chemotaxis in established tumors. Highfill et al. demonstrated enhanced tumor growth inhibition of established (day 7) rhabdomyosarcomas following PD-axis immune checkpoint blockade with

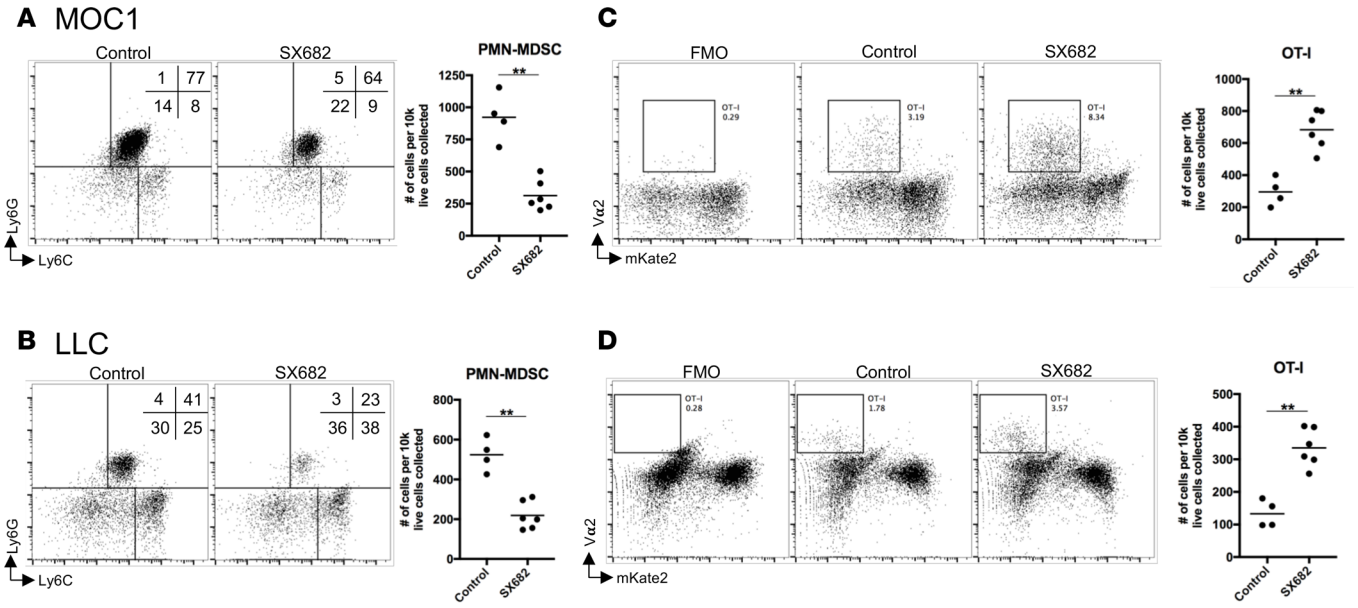

Figure 5. SX-682 results in greater tumor infiltration of adoptively transferred T cells. Day 15 tumors from RAG1$^{-/-}$ mice bearing MOC1 (**A**) or LLC (**B**) tumors engineered to express SIINFEKL were digested and assessed for infiltration of PMN-MDSCs after treatment with SX-682 or control chow starting on day 7. Representative dot plots of live CD45.2$^+$CD11b$^+$F4/80$^-$ cells on the left, with quantification on the right. RAG1$^{-/-}$ mice bearing MOC1 (**C**) or LLC (**D**) SIINFEKL–expressing tumors were treated with SX-682 or control chow on day 7 and treated with a single adoptive transfer of 1 × 10^6 OT-I T cells on day 10. Tumors were assessed for infiltration of Vα2$^+$ OT-I T cells 12 hours later. Representative dot plots of live cells on the left, quantification on the right. mKate2-positive cells are SIINFEKL-positive tumor cells. FMO, fluorescence minus one. Representative data from 1 of 2 independent assays with similar results shown. $^{**}P < 0.01$ by Student's *t* test.

CXCR2 blockade using a commercially available anti–mouse CXCR2 mAb (12). Work by Steele et al. revealed that a small-molecule inhibitor of CXCR2 could also enhance tumor growth inhibition following PD-axis immune checkpoint blockade in pancreatic adenocarcinoma (13). Similarly, Lu et al. demonstrated enhanced tumor growth inhibition of prostate cancer following combination PD-axis and CTLA-4 immune checkpoint blockade with SX-682 (14), the CXCR1/2 small-molecule inhibitor used in this study. Here, using SX-682 to block CXCR2$^+$ PMN-MDSC trafficking, we demonstrate enhanced tumor growth control or rejection of established tumors following both PD-axis immune checkpoint blockade and engineered adoptive T cell transfer. This suggests that immunosuppression mediated by PMN-MDSCs within the TME may be a common mechanism of resistance to both of these immunotherapeutic approaches.

The presence of immunosuppressive myeloid populations in the periphery and TME of patients with head and neck and lung cancers is well established by several independent groups (35–39). Greater accumulation of MDSCs within the periphery or tumors of patients with recurrent/metastatic head and neck or lung cancer correlates with decreased rates of response to PD-axis immune checkpoint blockade (9, 10). Yet other myeloid cell populations may also play a role in immunosuppression within the TME in human cancers, including polarized macrophages (reviewed in ref. 40). Here, we demonstrated that PMN-MDSCs are the dominant immunosuppressive myeloid cell subtype within MOC1 and LLC tumors. MOC1 CXCR1$^+$ macrophages were M2-polarized and immunosuppressive, though to a lesser degree than PMN-MDSCs, and LLC macrophages were M1-polarized and did not appear to suppress TIL function. This and other work suggest that intermodel variability in macrophage accumulation and suppressive capacity exists (41, 42). More broadly and from a translational standpoint, this suggests that individual tumors may harbor immunosuppressive immune cells from different lineages that harbor different receptors responsible for tumor trafficking. Despite peripheral macrophages from MOC1 and LLC tumors being CXCR1$^+$, SX-682 treatment did not alter tumor trafficking of macrophages in either model. Macrophages in these models may rely on multiple redundant chemokine signaling pathways for tumor trafficking such as CSF1R (43, 44). Our data suggest that CSF1R may be the dominant chemokine receptor expressed on macrophages in these models. Tumor immune profiling indicative of a PMN-MDSC–rich or macrophage-rich TME could serve as a biomarker for determining which chemokine signaling axis inhibitor to use in combination with immunotherapy. Validation of this approach requires further study.

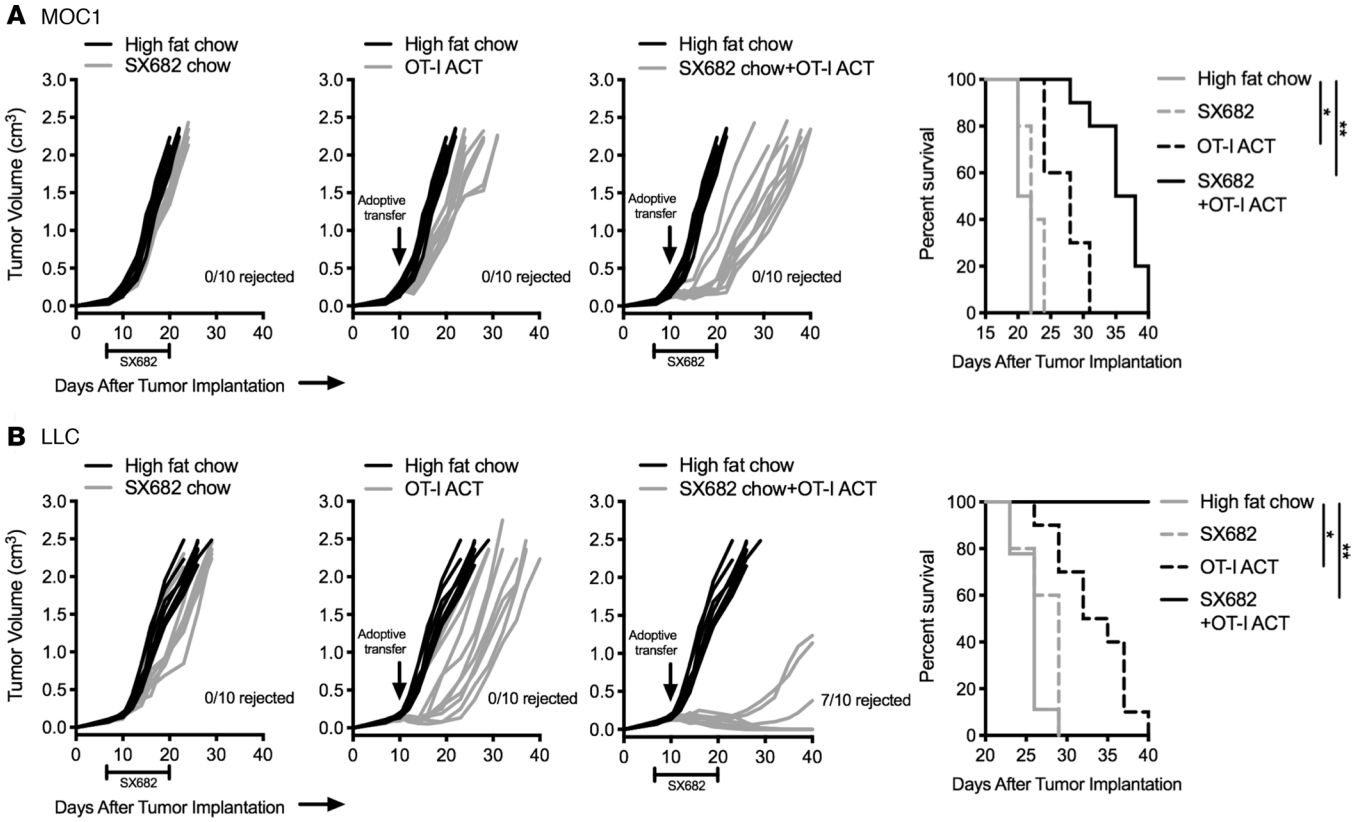

Figure 6. SX-682 enhances tumor control or rejection following adoptive transfer of antigen-specific T cells. RAG1$^{-/-}$ mice bearing MOC1 (**A**) or LLC (**B**) SIINFEKL–expressing tumors were treated with SX-682 or control chow on day 7 and treated with a single adoptive transfer of 1 × 10^6 OT-I T cells (OT-1 ACT) on day 10. Mice were followed for primary tumor growth (left) and survival (right). Cumulative results from 2 independent experiments shown. *P < 0.05; **P < 0.01 by log-rank (Mantel-Cox) analysis.

Targeting CXCR2 may be the ideal approach for selectively abrogating PMN-MDSC trafficking into tumors. Expression of CXCR2 on both murine and human neutrophilic cells appears to be universal (6). CXCR2 is also expressed on normal neutrophils, but inhibition of CXCR2 with a small-molecule inhibitor does not appear to suppress neutrophil responses to bacteria, and treatment-related reductions in blood neutrophil counts with CXCR2 blockade appear to be temporary, with rapid rebound following cessation of drug (45, 46). Timing of chemokine receptor inhibition may also be important. We previously demonstrated that in the MOC1 model, PMN-MDSCs are relatively low and TILs are relatively high on day 10 of tumor progression (11). With progression from day 10 to 20, PMN-MDSCs increase and TILs decrease. Here, we demonstrated that SX-682 started on day 10 resulted in increased TIL accumulation within tumors on day 25, but this was not observed when treatment started on day 20, suggesting that earlier inhibition of immunosuppressive cell trafficking may more effectively rescue effector immune cells. Other chemokine receptors, such as CXCR4, are also expressed on bone marrow and peripheral neutrophilic cells and may be important for trafficking into tumors (47). However, mounting evidence suggests that CXCR4 signaling acts as an important retention signal for neutrophilic cells in the bone marrow, and that CXCR4 inhibition may mobilize these cells from the marrow into circulation (48, 49). CXCR4 is also expressed at high levels on T cells (50). Given these data, CXCR2 inhibition likely offers the most selective inhibition of neutrophilic cell trafficking into tumors.

The mechanism of action of SX-682 described here appeared to be limited to disruption of CXCR2-mediated PMN-MDSC trafficking, despite the fact that both CXCR1 and CXCR2 are expressed on MOC1 and LLC tumor cells. SX-682 treatment had little or no effects on MOC1 or LLC tumor cell proliferation, viability, or direct susceptibility to T cell killing in vitro. SX-682 monotherapy also had no effect on primary tumor growth in vivo in both models studied here. Other studies have demonstrated, however, that inhibition of CXCR1 and CXCR2 signaling in carcinoma cells can impact invasive capacity, survival of stem-like cells, epithelial-to-mesenchymal transition (EMT), and resistance to tyrosine kinase inhibitors (51–54). The tumor

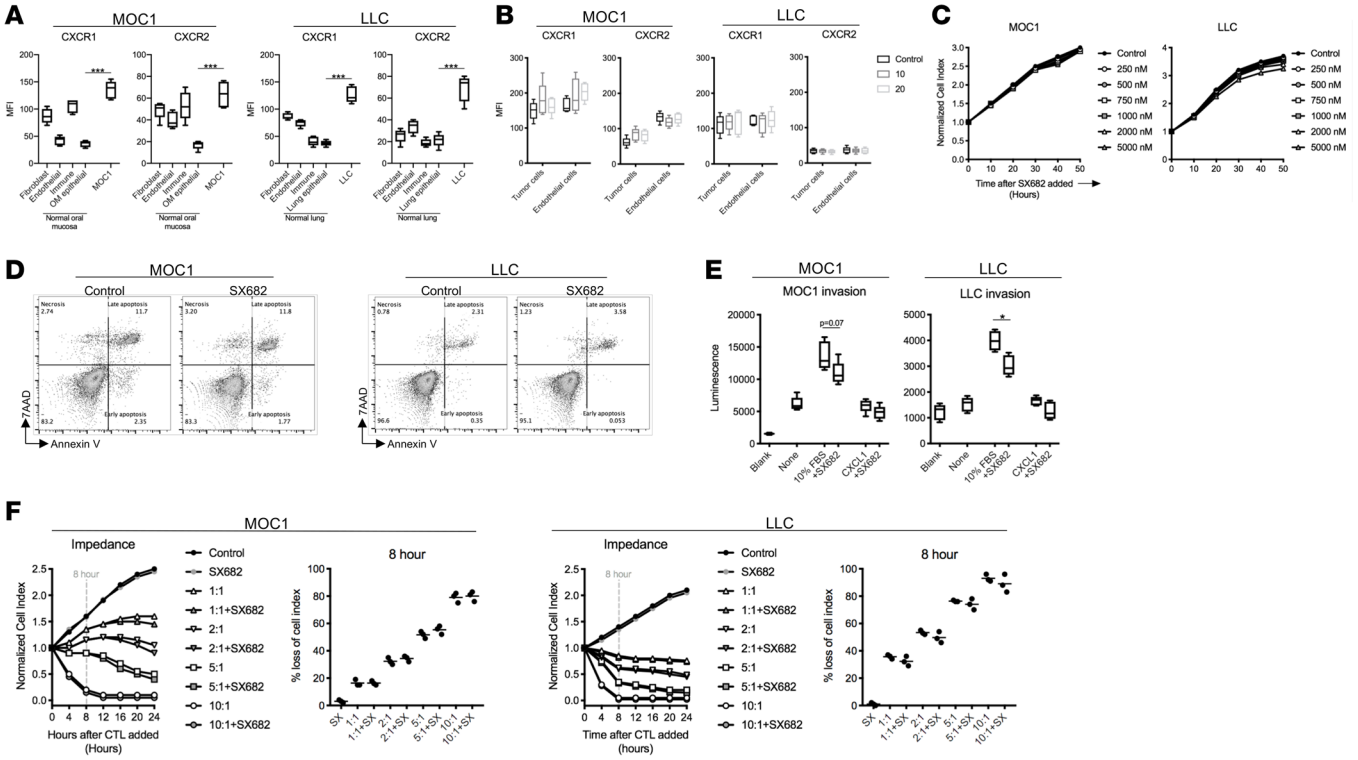

Figure 7. SX-682 treatment effect is not due to direct alteration of tumor cell viability, invasive capacity, or immunogenicity. (**A**) MOC1 or LLC cells were assessed for CXCR1 or CXCR2 expression by flow cytometry, compared to fibroblasts, endothelial, immune or epithelial cells from MOC1 or LLC tumors in vivo. Live CD45.2$^-$CD31$^-$PDGFR$^-$ oral mucosal epithelial cells and lung epithelial cells were used as comparators for MOC1 and LLC, respectively. (**B**) CXCR1 and CXCR2 expression on day 25 CD45.2$^-$CD31$^-$PDGFR$^-$ MOC1 or LLC tumor cells following SX-682 treatment beginning on day 10 or 20 after tumor implantation was assessed by flow cytometry. (**C**) MOC1 or LLC cells were plated in increasing doses of SX-682 and evaluated for alteration in viability via impedance analysis. (**D**) MOC1 or LLC cells were exposed to SX-682 (1 μM for 24 hours) and assessed for induction of apoptosis via flow cytometry. (**E**) Extracellular matrix invasion of MOC1 or LLC cells was assessed using 10% FBS (positive control) or CXCL1 (50 ng/ml) as the chemoattractant in the presence or absence of SX-682 (1 μM). (**F**) MOC1 or LLC cells expressing SIINFEKL were exposed to activated OT-I T cells in the presence or absence of SX-682 (cells plated in 1 μM) and T cell killing was assessed via impedance analysis. Representative impedance plots on the left, with quantification at 8 hours on the right. Representative data from 1 of at least 2 independent assays with similar results shown. *$P < 0.05$; ***$P < 0.001$ by Student's *t* test.

cell–intrinsic determinants of the CXCR1 or CXCR2 contribution to these biological processes are unclear but may be related to the underlying EMT status of the tumor cells. Invasion through an ECM does not appear to be driven by CXCR2 in epithelial cells like LLC and MOC1, whereas chemokine signaling may contribute to migration and/or invasion in more mesenchymal cells (54). This requires further study. Regardless, our results suggest that CXCR2 blockade, through modulation of the TME, can enhance responses to immunotherapy independent of directly altered CXCR1/2 signaling within tumor cells.

In summary, this work demonstrated the ability of SX-682 to enhance responses to PD-axis immune checkpoint blockade and adoptive transfer of engineered T cells through selective inhibition of CXCR2$^+$ PMN-MDSC trafficking into tumors. These data suggest that tumor PMN-MDSCs may be important modulators of response to both forms of immunotherapy. As with any preclinical model, these results require validation in carefully controlled clinical trials. Head and neck and lung SCCs harbor heavy myeloid cell infiltration and display limited responses despite expression of immune checkpoints, indicating that CXCR2 inhibition may be beneficial and carry the potential to enhance responses to T cell–based immunotherapies in patients with these cancers.

Methods

Cells, treatments, and animal studies. MOC1 cells from the same stock that has been genomically characterized were obtained from Ravindra Uppaluri (Washington University, St. Louis, Missouri, USA) and LLC cells were obtained from James Hodge (National Cancer Institute) (55). Cells were used at low passage number, serially tested for murine pathogens and mycoplasma, and cultured as described previously (56). SX-682 was obtained

under a Cooperative Research and Development Agreement with Syntrix Pharmaceuticals. Recombinant murine CXCL1 was purchased from R&D Systems. Cells expressing $OVA_{257–264}$ (SIINFEKL) were generated as described previously (57). Peripheral blood was sampled via cardiac puncture. Tumors were established by flank subcutaneous injections of MOC1 (5×10^6 cells) or LLC (2×10^6 cells) or their corresponding SIINFEKL-expressing variants in 30% Matrigel (Trevigen). SX-682 was formulated in high-fat chow by Research Diets, Inc. Anti–PD-1 mAb (clone RMP1-14) and isotype control (clone 2A3) were purchased from BioXCell. For some experiments, $CD8^+$ cells were depleted in vivo via i.p. injection of antibody (clone YTS 169.4, BioXCell). OT-I CTLs were generated ex vivo as described previously (57) and adoptively transferred via i.p. injection.

Flow cytometry. Only fresh cells or tumor, spleen, bone marrow, oral mucosa, or lung tissues prepared into single-cell suspensions, as described previously (11), were analyzed. Nonspecific staining was minimized with Fc receptor (FcR) blockade. Primary conjugated antibodies were purchased from Biolegend, BD Pharmingen, or eBioscience and applied for 30–60 minutes. Dead cells were excluded via viability dye staining and a fluorescence-minus-one technique was used to validate specific staining of all antibody combinations (58). Apoptosis was assessed using the Annexin V Apoptosis Detection Kit (eBioscience) per the manufacturer's protocol. For some experiments, cells were fixed and permeabilized for intranuclear (Ki67) staining using the FoxP3 Transcription Factor Staining Buffer Set (eBioscience) per the manufacturer's recommendations. All analyses were performed on a BD FACSCanto or BD Fortessa analyzer running FACSDiva software and interpreted using FlowJo (vX10.0.7r2).

TIL culture. Day 14 MOC1 or LLC tumors were harvested, minced into 1-mm fragments, and plated in RPMI1640-based media with recombinant murine IL-2 (rmIL-2; 100 U/ml). After 72 hours, tumor fragments were removed. TILs were cultured in rmIL-2 for an additional 3 to 10 days, replenishing fresh media every 48 hours.

Myeloid cell sorting. MOC1 or LLC tumors were digested into single-cell suspensions and run in a 40%/80% Percoll gradient. The leukocyte band was harvested and $Ly6G^{hi}$ cells or $F4/80^+$ cells were sorted using the Anti-Ly6G MicroBead Kit and Anti-F4/80 MicroBead Kit, respectively, on an AutoMACS Pro (Miltenyi Biotec) per the manufacturer's recommendations.

PMN-MDSC IFN-γ suppression assay. $CD3^+$ T cell were isolated from day 7 cultured TILs via negative magnetic selection using the Pan T cell Selection Kit II on the AutoMACS Pro (Miltenyi Biotec). T cells were plated into appropriate wells of a 24-well plate coated with anti-CD3 and anti-CD28 mAbs as previously described (59). $Ly6G^{hi}$ cells were isolated as described previously (59). T cells (1×10^5) with or without $Ly6G^{hi}$ cells (3×10^5) were plated for 24 hours. For the final 6 hours of the incubation, brefeldin (5.3 mM) was added. Cells were fixed and permeabilized with the Intracellular Fix and Perm Set (eBioscience) per the manufacturer's recommendations and with anti–IFN-γ antibody in preparation for flow cytometry.

Impedance analysis. MOC1 or LLC cells (1×10^4 cells/well) were plated in the presence or absence of DMSO control or SX-682. In other experiments designed to measure potential abrogation of cultured TIL-mediated antigen-specific cytotoxicity, MOC1 or LLC cells were plated and allowed to gain impedance for 24–48 hours. Cultured TILs were then added at a 10:1 effector/target (E/T) ratio in the presence or absence of tumor $Ly6G^{hi}$ myeloid cells or $F4/80^+$ myeloid cells (3:1 E/T ratio to the TILs). TILs, $Ly6G^{hi}Ly6C^{lo}$ myeloid cells, or $F4/80^+$ myeloid cells were combined and incubated together for 2 hours before addition to the impedance plate. Impedance experiments were performed using 96-well E-Plates (ACEA Biosciences) and changes in impedance were recorded using the xCELLigence Real-Time Cell Analysis (RTCA) platform per the manufacturer's recommendations. For each plot, the *y* axis is the cell index and the *x* axis is time in hours. Triton X-100 (0.2%) was added to some wells to induce total cell lysis. The percentage loss of cell index for a given time point was calculated using the following: 1 – (experimental cell index/control cell index).

ELISA. ELISA kits were purchased from R&D Systems and used per the manufacturer's recommendations.

qRT-PCR. Quantitative reverse transcription PCR (qRT-PCR) was performed as previously described (57). CXCL1 and GAPDH primers were purchased from Thermo Fisher Scientific.

Invasion assay. The QCM ECMatrix Cell Invasion Assay was purchased from EMD Millipore and used per the manufacturer's recommendations. Recombinant murine CXCL1 was purchased from R&D Systems.

Statistics. Tests of significance between pairs of data are reported as *P* values, derived using a Student's *t* test with a 2-tailed distribution and calculated at 95% confidence. Comparison of multiple sets of data was achieved with analysis of variance (ANOVA) with Tukey's multiple-comparisons test. Survival analysis was determined by log-rank (Mantel-Cox) analysis. All error bars indicate standard deviation. Statistical significance was set to $P < 0.05$. All analysis was performed using GraphPad Prism v7.

Study approval. All in vivo treatments were approved by the NIH Animal Care and Use Committee.

Author contributions

LS, JS, CP, and CTA designed the experiments. LS, PEC, YR, PP, JF, SG, RD, CS, and LAH conducted the experiments. LS, PEC, YR, PP, JF, SG, RD, CS, and LAH acquired data. LS, PEC, YR, PP, JF, SG, RD, CS, LAH, CVW, JS, CP, and CTA analyzed data. JS, CP, and CTA provided reagents. DM and JZ analyzed data and provided reagents. LS, CVW, JS, CP, and CTA wrote the manuscript.

Acknowledgments

The authors thank Nicole Schmitt and Rajarsi Mandal for their critical review of this work. This work was supported by the Intramural Research Program of the NIH National Institute on Deafness and Other Communication Disorders (project number ZIA-DC000087).

Address correspondence to: Clint T. Allen; 10 Center Drive, Room 7N240C, Bethesda, Maryland, USA. Phone: 301.827.5620; Email: clint.allen@nih.gov.

1. Davis RJ, Van Waes C, Allen CT. Overcoming barriers to effective immunotherapy: MDSCs, TAMs, and Tregs as mediators of the immunosuppressive microenvironment in head and neck cancer. *Oral Oncol*. 2016;58:59–70.
2. Campbell JD, et al. Genomic, pathway network, and immunologic features distinguishing squamous carcinomas. *Cell Rep*. 2018;23(1):194–212.e6.
3. Redon R, Muller D, Caulee K, Wanherdrick K, Abecassis J, du Manoir S. A simple specific pattern of chromosomal aberrations at early stages of head and neck squamous cell carcinomas: PIK3CA but not p63 gene as a likely target of 3q26-qter gains. *Cancer Res*. 2001;61(10):4122–4129.
4. Yang X, et al. ΔNp63 versatilely regulates a broad NF-κB gene program and promotes squamous epithelial proliferation, migration, and inflammation. *Cancer Res*. 2011;71(10):3688–3700.
5. Du J, et al. Epidermal overexpression of transgenic ΔNp63 promotes type 2 immune and myeloid inflammatory responses and hyperplasia via NF-κB activation. *J Pathol*. 2014;232(3):356–368.
6. Liu Q, et al. The CXCL8-CXCR1/2 pathways in cancer. *Cytokine Growth Factor Rev*. 2016;31:61–71.
7. Gabrilovich DI, Ostrand-Rosenberg S, Bronte V. Coordinated regulation of myeloid cells by tumours. *Nat Rev Immunol*. 2012;12(4):253–268.
8. Gabrilovich DI. Myeloid-derived suppressor cells. *Cancer Immunol Res*. 2017;5(1):3–8.
9. Seiwert TY, et al. Correlation of constitutive PD-1 resistance in HNC with GM-CSF expression and presence of myeloid derived suppressor cells (MDSCs). *J Clin Oncol*. 2017;35(suppl 15):6049.
10. Delaunay M, et al. Baseline circulating myeloid-derived suppressor cells response to PD-1 inhibitor in non-small cell lung cancer patients. *J Clin Oncol*. 2018;35(suppl 5):145.
11. Clavijo PE, et al. Resistance to CTLA-4 checkpoint inhibition reversed through selective elimination of granulocytic myeloid cells. *Oncotarget*. 2017;8(34):55804–55820.
12. Highfill SL, et al. Disruption of CXCR2-mediated MDSC tumor trafficking enhances anti-PD1 efficacy. *Sci Transl Med*. 2014;6(237):237ra67.
13. Steele CW, et al. CXCR2 inhibition profoundly suppresses metastases and augments immunotherapy in pancreatic ductal adenocarcinoma. *Cancer Cell*. 2016;29(6):832–845.
14. Lu X, et al. Effective combinatorial immunotherapy for castration-resistant prostate cancer. *Nature*. 2017;543(7647):728–732.
15. Davis RJ, et al. Anti-PD-L1 efficacy can be enhanced by inhibition of myeloid-derived suppressor cells with a selective inhibitor of PI3Kδ/γ. *Cancer Res*. 2017;77(10):2607–2619.
16. Scholten DJ, et al. Pharmacological modulation of chemokine receptor function. *Br J Pharmacol*. 2012;165(6):1617–1643.
17. Bronte V, et al. Recommendations for myeloid-derived suppressor cell nomenclature and characterization standards. *Nat Commun*. 2016;7:12150.
18. Rose JJ, Foley JF, Murphy PM, Venkatesan S. On the mechanism and significance of ligand-induced internalization of human neutrophil chemokine receptors CXCR1 and CXCR2. *J Biol Chem*. 2004;279(23):24372–24386.
19. Dominguez C, McCampbell KK, David JM, Palena C. Neutralization of IL-8 decreases tumor PMN-MDSCs and reduces mesenchymalization of claudin-low triple-negative breast cancer. *JCI Insight*. 2017;2(21):94296.
20. McColl SR, Clark-Lewis I. Inhibition of murine neutrophil recruitment in vivo by CXC chemokine receptor antagonists. *J Immunol*. 1999;163(5):2829–2835.
21. Loukinova E, et al. Growth regulated oncogene-alpha expression by murine squamous cell carcinoma promotes tumor growth, metastasis, leukocyte infiltration and angiogenesis by a host CXC receptor-2 dependent mechanism. *Oncogene*. 2000;19(31):3477–3486.
22. Li J, et al. Tumor cell-intrinsic factors underlie heterogeneity of immune cell infiltration and response to immunotherapy. *Immunity*. 2018;49(1):178–193.e7.
23. Tumeh PC, et al. PD-1 blockade induces responses by inhibiting adaptive immune resistance. *Nature*. 2014;515(7528):568–571.
24. Rosenberg SA, Restifo NP, Yang JC, Morgan RA, Dudley ME. Adoptive cell transfer: a clinical path to effective cancer immunotherapy. *Nat Rev Cancer*. 2008;8(4):299–308.

25. Brahmer J, et al. Nivolumab versus docetaxel in advanced squamous-cell non-small-cell lung cancer. *N Engl J Med*. 2015;373(2):123–135.
26. Ferris RL, et al. Nivolumab for Recurrent squamous-cell carcinoma of the head and neck. *N Engl J Med*. 2016;375(19):1856–1867.
27. Goff SL, et al. Randomized, prospective evaluation comparing intensity of lymphodepletion before adoptive transfer of tumor-infiltrating lymphocytes for patients with metastatic melanoma. *J Clin Oncol*. 2016;34(20):2389–2397.
28. Stevanović S, et al. Complete regression of metastatic cervical cancer after treatment with human papillomavirus-targeted tumor-infiltrating T cells. *J Clin Oncol*. 2015;33(14):1543–1550.
29. Sackstein R, Schatton T, Barthel SR. T-lymphocyte homing: an underappreciated yet critical hurdle for successful cancer immunotherapy. *Lab Invest*. 2017;97(6):669–697.
30. Keane MP, Belperio JA, Xue YY, Burdick MD, Strieter RM. Depletion of CXCR2 inhibits tumor growth and angiogenesis in a murine model of lung cancer. *J Immunol*. 2004;172(5):2853–2860.
31. Mestas J, Burdick MD, Reckamp K, Pantuck A, Figlin RA, Strieter RM. The role of CXCR2/CXCR2 ligand biological axis in renal cell carcinoma. *J Immunol*. 2005;175(8):5351–5357.
32. Jamieson T, et al. Inhibition of CXCR2 profoundly suppresses inflammation-driven and spontaneous tumorigenesis. *J Clin Invest*. 2012;122(9):3127–3144.
33. Chao T, Furth EE, Vonderheide RH. CXCR2-dependent accumulation of tumor-associated neutrophils regulates T-cell immunity in pancreatic ductal adenocarcinoma. *Cancer Immunol Res*. 2016;4(11):968–982.
34. Katoh H, Wang D, Daikoku T, Sun H, Dey SK, Dubois RN. CXCR2-expressing myeloid-derived suppressor cells are essential to promote colitis-associated tumorigenesis. *Cancer Cell*. 2013;24(5):631–644.
35. Lang S, et al. Clinical relevance and suppressive capacity of human myeloid-derived suppressor cell subsets. *Clin Cancer Res*. 2018;24(19):4834–4844.
36. Vasquez-Dunddel D, et al. STAT3 regulates arginase-I in myeloid-derived suppressor cells from cancer patients. *J Clin Invest*. 2013;123(4):1580–1589.
37. Ortiz ML, Lu L, Ramachandran I, Gabrilovich DI. Myeloid-derived suppressor cells in the development of lung cancer. *Cancer Immunol Res*. 2014;2(1):50–58.
38. Zhang G, et al. A novel subset of B7-H3^{+}CD14^{+}HLA-DR$^{-/low}$ myeloid-derived suppressor cells are associated with progression of human NSCLC. *Oncoimmunology*. 2015;4(2):e977164.
39. Huang A, Zhang B, Wang B, Zhang F, Fan KX, Guo YJ. Increased CD14(+)HLA-DR (-/low) myeloid-derived suppressor cells correlate with extrathoracic metastasis and poor response to chemotherapy in non-small cell lung cancer patients. *Cancer Immunol Immunother*. 2013;62(9):1439–1451.
40. Noy R, Pollard JW. Tumor-associated macrophages: from mechanisms to therapy. *Immunity*. 2014;41(1):49–61.
41. Mitchem JB, et al. Targeting tumor-infiltrating macrophages decreases tumor-initiating cells, relieves immunosuppression, and improves chemotherapeutic responses. *Cancer Res*. 2013;73(3):1128–1141.
42. Hagemann T, et al. "Re-educating" tumor-associated macrophages by targeting NF-kappaB. *J Exp Med*. 2008;205(6):1261–1268.
43. Peranzoni E, et al. Macrophages impede CD8 T cells from reaching tumor cells and limit the efficacy of anti-PD-1 treatment. *Proc Natl Acad Sci USA*. 2018;115(17):E4041–E4050.
44. Ren G, et al. CCR2-dependent recruitment of macrophages by tumor-educated mesenchymal stromal cells promotes tumor development and is mimicked by TNFα. *Cell Stem Cell*. 2012;11(6):812–824.
45. Jurcevic S, Humfrey C, Uddin M, Warrington S, Larsson B, Keen C. The effect of a selective CXCR2 antagonist (AZD5069) on human blood neutrophil count and innate immune functions. *Br J Clin Pharmacol*. 2015;80(6):1324–1336.
46. O'Byrne PM, et al. Efficacy and safety of a CXCR2 antagonist, AZD5069, in patients with uncontrolled persistent asthma: a randomised, double-blind, placebo-controlled trial. *Lancet Respir Med*. 2016;4(10):797–806.
47. Du R, et al. HIF1alpha induces the recruitment of bone marrow-derived vascular modulatory cells to regulate tumor angiogenesis and invasion. *Cancer Cell*. 2008;13(3):206–220.
48. Eash KJ, Greenbaum AM, Gopalan PK, Link DC. CXCR2 and CXCR4 antagonistically regulate neutrophil trafficking from murine bone marrow. *J Clin Invest*. 2010;120(7):2423–2431.
49. Suratt BT, et al. Role of the CXCR4/SDF-1 chemokine axis in circulating neutrophil homeostasis. *Blood*. 2004;104(2):565–571.
50. Peng W, et al. Transduction of tumor-specific T cells with CXCR2 chemokine receptor improves migration to tumor and antitumor immune responses. *Clin Cancer Res*. 2010;16(22):5458–5468.
51. Khurram SA, Bingle L, McCabe BM, Farthing PM, Whawell SA. The chemokine receptors CXCR1 and CXCR2 regulate oral cancer cell behaviour. *J Oral Pathol Med*. 2014;43(9):667–674.
52. Ginestier C, et al. CXCR1 blockade selectively targets human breast cancer stem cells in vitro and in xenografts. *J Clin Invest*. 2010;120(2):485–497.
53. Fernando RI, Castillo MD, Litzinger M, Hamilton DH, Palena C. IL-8 signaling plays a critical role in the epithelial-mesenchymal transition of human carcinoma cells. *Cancer Res*. 2011;71(15):5296–5306.
54. Fernando RI, Hamilton DH, Dominguez C, David JM, McCampbell KK, Palena C. IL-8 signaling is involved in resistance of lung carcinoma cells to erlotinib. *Oncotarget*. 2016;7(27):42031–42044.
55. Onken MD, et al. A surprising cross-species conservation in the genomic landscape of mouse and human oral cancer identifies a transcriptional signature predicting metastatic disease. *Clin Cancer Res*. 2014;20(11):2873–2884.
56. Cash H, et al. mTOR and MEK1/2 inhibition differentially modulate tumor growth and the immune microenvironment in syngeneic models of oral cavity cancer. *Oncotarget*. 2015;6(34):36400–36417.
57. Sun L, et al. WEE1 kinase inhibition reverses G2/M cell cycle checkpoint activation to sensitize cancer cells to immunotherapy. *Oncoimmunology*. 2018;7(10):e1488359.
58. Herzenberg LA, Tung J, Moore WA, Herzenberg LA, Parks DR. Interpreting flow cytometry data: a guide for the perplexed. *Nat Immunol*. 2006;7(7):681–685.
59. Davis RJ, Silvin C, Allen CT. Avoiding phagocytosis-related artifact in myeloid derived suppressor cell T-lymphocyte suppression assays. *J Immunol Methods*. 2017;440:12–18.